SUPPLEMENTAL MATERIAL

Supplemental Methods

I_{Ks} and I_{to} heterogeneities in 2D tissue model. We simulated two types of heterogeneities in the 2D tissue model in Fig.1. In the first type (Figs. 1 A and B), we used transmural heterogeneities in I_{Ks} and I_{to} with the maximum conductances G_{Ks} and G_{to} being the following distributions:

$$G_{Ks}(y) = \begin{cases} 0.5G_{Ks}, & y < L/2 \\ [\frac{2}{L}\left(y - \frac{L}{2}\right) + 0.5]G_{Ks}, & \frac{L}{2} < y < 3L/4 \\ G_{Ks}, & y > 3L/4 \end{cases} \quad \text{(S1)}$$

and

$$G_{to}(y) = \begin{cases} 0, & y < L/2 \\ \frac{4}{L}\left(y - \frac{L}{2}\right)G_{to}, & \frac{L}{2} < y < 3L/4 \\ G_{to}, & y > 3L/4 \end{cases} \quad \text{(S2)}$$

where L=256 cells, which is the cable length. G_{Ks} in Eq.S1 is control value in original model, i.e., G_{Ks}=0.433 mS/cm^2 and G_{to} in Eq.S2 is the largest value as marked on each panel in Figs. 1 A and B.

In the second type (Fig.1C), in addition to the transmural heterogeneities in G_{Ks} and G_{to}, we also added a G_{to} heterogeneity in the longitudinal direction by setting G_{Ks} and G_{to} as follows:

$$G_{Ks}(x,y) = \begin{cases} 0.5G_{Ks}, & y \le L/2 \\ G_{Ks}, & y > L/2 \end{cases} \quad \text{(S3)}$$

and

$$G_{to}(x,y) = \begin{cases} 0, & y \le L/2 \\ \frac{3x}{L} & y > L/2 \end{cases} \quad \text{(S4)}$$

where L=512 cells.

Pseudo-ECG. The pseudo-ECG was calculated as:

$$ECG = \iint \mathbf{D}\nabla V \cdot \nabla\left(\frac{1}{r}\right) dxdy \quad \text{(S5)}$$

where $r = \sqrt{(x-x_p)^2 + (y-y_p)^2 + z_p^2}$ and (x_p, y_p, z_p)=(1.92 cm, 0.864 cm, 0.15 cm) is the location of the pseudo-ECG electrode.

Numerical methods. An explicit Euler method with a fixed time step $\Delta t = 0.01$ ms was used for simulations of both the 1D cable (Eq.1) and the 2D tissue (Eq.2). In the 1D cable simulations, we used D=0.001 cm^2/ms and Δx=0.015 cm. For the 2D tissue simulating the endo-epi heterogeneities for ECG morphologies and P2R, we used D_x=0.001 cm^2/ms, Δx=0.015 cm, D_y=0.001/16 cm^2/ms, and Δy=0.015/4 cm. For the spiral wave stabilities, we simulated a homogeneous tissue with D_x=D_y=0.001 cm^2/ms and Δx=Δy=0.015 cm. The same numerical methods were used for the 1994 Luo and Rudy model and the 2004 ten Tusscher et al human model. All the codes were programed in CUDA C++, and simulations were performed on NVIDIA Tesla K80 GPU cards (NVIDIA, Santa Clara, CA).

Supplemental Table

Table I. **The female-to-male ratios of the maximum conductance of ionic currents and gap junction conductance.** The values were based on the data from previous studies [30,33]. Except I_{to}, there were no epi-to-endo heterogeneities in currents in the 1D cable model. In other words, the female-to-male ratios were uniform in the cable, no epi-to-endo heterogeneities except I_{to}. We did the same simulations as in Fig.8 and Fig.X using the same epi-to-endo heterogeneities in female-to-male ratios as in Yang et al [30], we only observed small differences from the ones shown in Fig.8 and Fig.X.

	P_{Ca}	G_{Ks}	G_{Kr}	G_{to}	G_{K1}	G_{NaK}	D
Female/male	1.5	0.85	0.85	0.5	0.8	0.75	0.65

Supplemental Figures

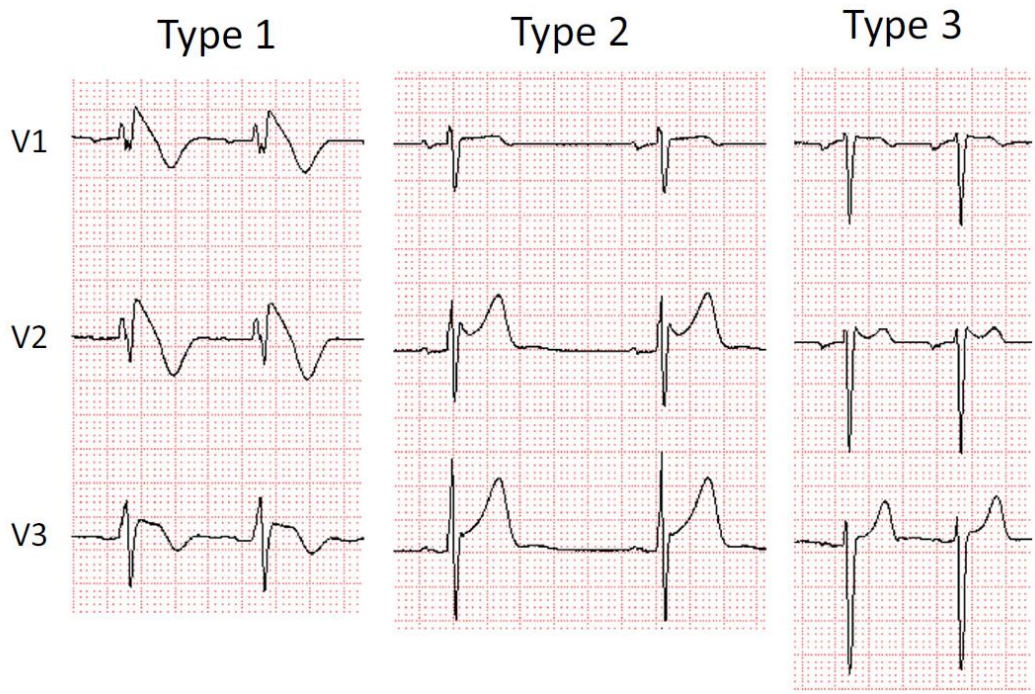

Figure I. **Three types of characteristic ECGs associated with BrS,** reproduced from Antzelevitch et al [7] with permission.

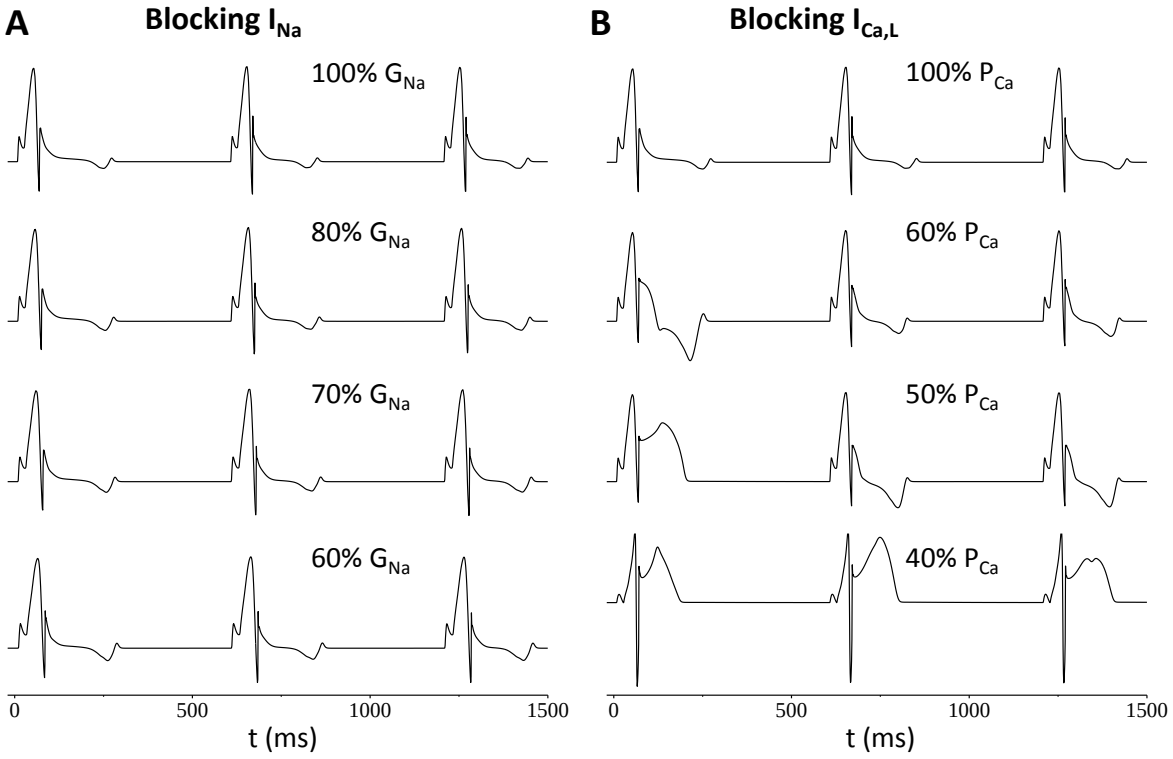

Figure II. Promotion of type 1 (coved) ECG by blocking I_{Na} or $I_{Ca,L}$. Simulations were done the same way as for Fig.1A in the main text. **A**. ECGs at different levels of I_{Na} as marked. **B**. ECGs at different levels of $I_{Ca,L}$ as marked. All parameters were the same as in Fig.1A with G_{to}=1 mS/cm^2.

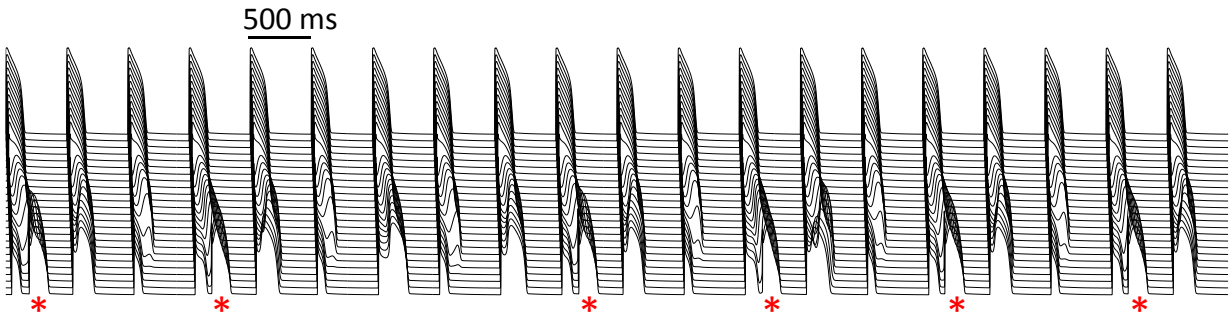

Figure III. An example of time-space plot of voltage under periodic pacing with PCL=500 ms from Fig.3A in the main text with γ=0 and G_{to}=1.5 mS/cm^2. "*" marks the PVCs/P2Rs.

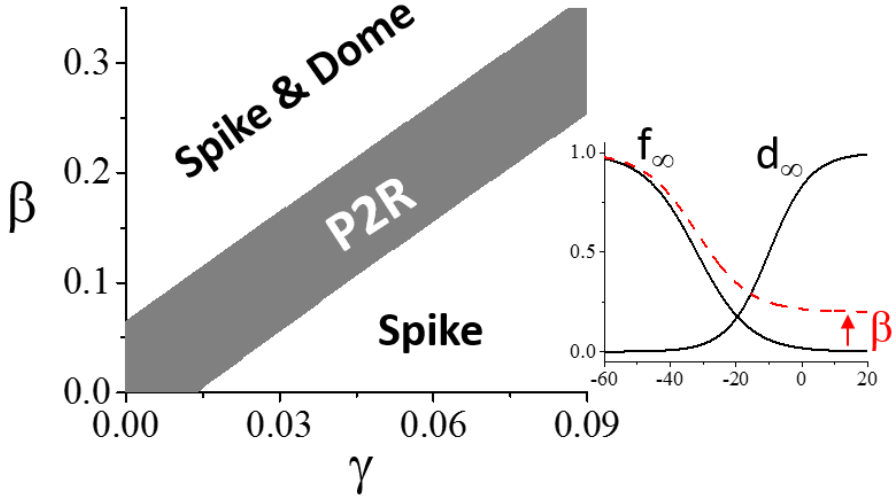

Figure IV. **Effects of late $I_{Ca,L}$ on P2R in 1D cable simulations using the Luo and Rudy AP model**. The simulations were done under the same condition as for Fig.6 in the main text. Shown is the P2R region versus γ and β. γ is the parameter controlling the late component of I_{to}. β is the parameter controlling the late component of $I_{Ca,L}$ by changing the steady-state inaction (f_∞) as: $f_{\infty,new} = \beta + (1-\beta)f_\infty$ (as indicated in the inset). The effect of increasing late I_{to} (γ) on P2R is compensated by increasing the late $I_{Ca,L}$ (β), similar to shifting f_∞ as shown in Fig.7E. P_{Ca}=0.000594 cm/s and G_{to}=1.75 mS/cm^2.

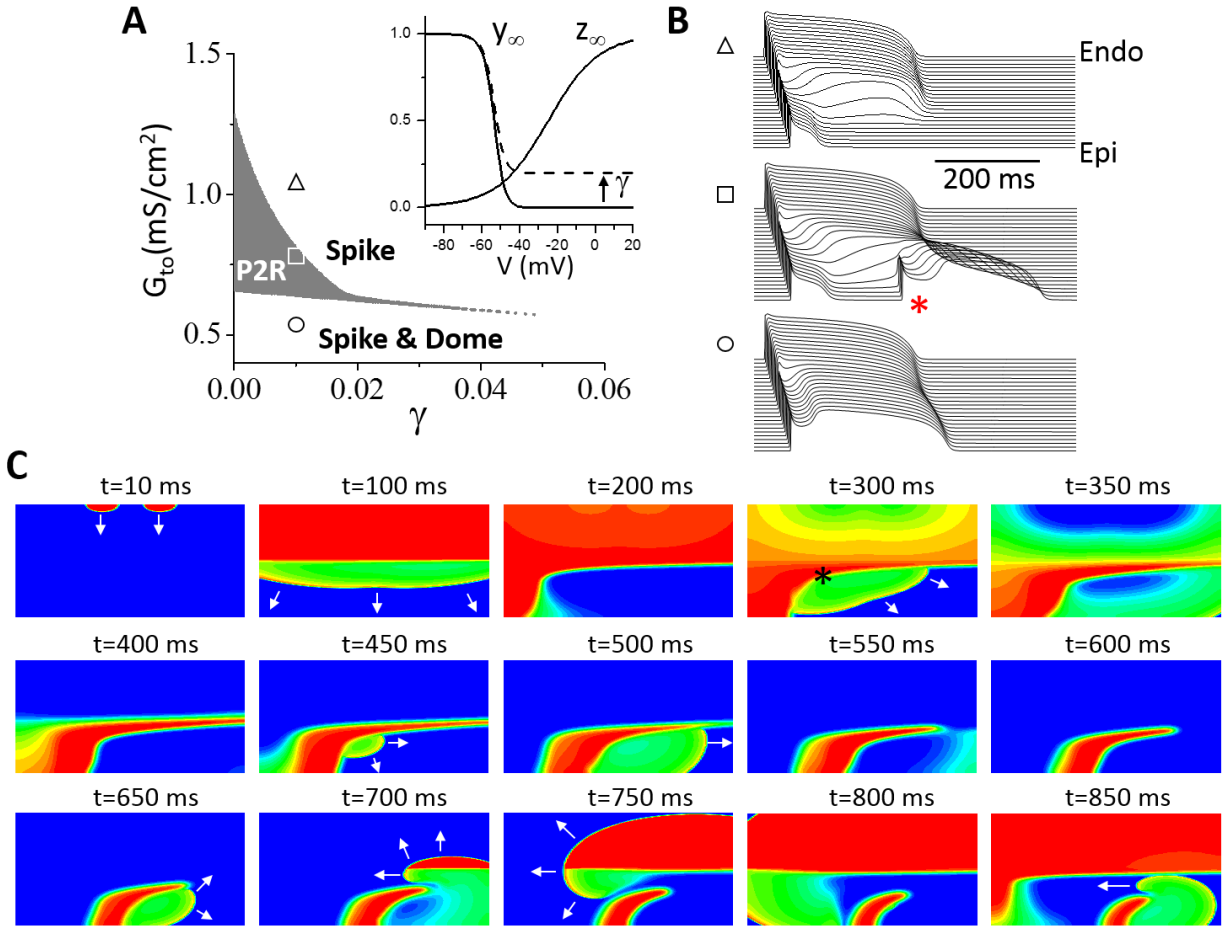

Figure V. Effects of late I_{to} on P2R in tissue using the ten Tusscher et al human ventricular AP model. **A**. P2R region versus G_{to} and γ. γ (Eq.4) controls the level of incomplete inactivation of the steady state as indicated in the inset. The simulations were done in the same way as for Fig.2A in the main text. **B**. Time-space plots of voltage from the three parameter locations marked in A. **C**. Wave dynamics in a heterogeneous 2D tissue as for Fig.1C in main text. Shown are voltage snapshots at different time points. Arrows indicate propagating wavefronts. A wave elicited from two stimulus sites (t=10 ms) propagated from the endocardium to epicardium (t=100 ms). Due to the early repolarization in the lower-right quadrant, P2R occurs (t=300 ms, marked by *), propagates toward the tissue boundary and disappears (t=350 ms and 400 ms). The repolarization pattern remains heterogeneous (t=400 ms) and a new P2R occurs (t=450 ms). Additional new P2Rs occur at t=650 and 850 ms. Tissue size is 7.68 cm x 1.92 cm. See Supplemental Movie II for detailed wave dynamics. $G_{Ks}(x,y) = \begin{cases} 0.5G_{Ks} & y \le L/2 \\ G_{Ks} & y > L/2 \end{cases}$ with the control G_{Ks}=0.245 mS/cm^2, and $G_{to}(x,y) = \begin{cases} 0, & y \le L/2. \\ 0.5 + \frac{2}{L}\left(x - \frac{L}{2}\right), & y > L/2. \end{cases}$ L=512 cells.

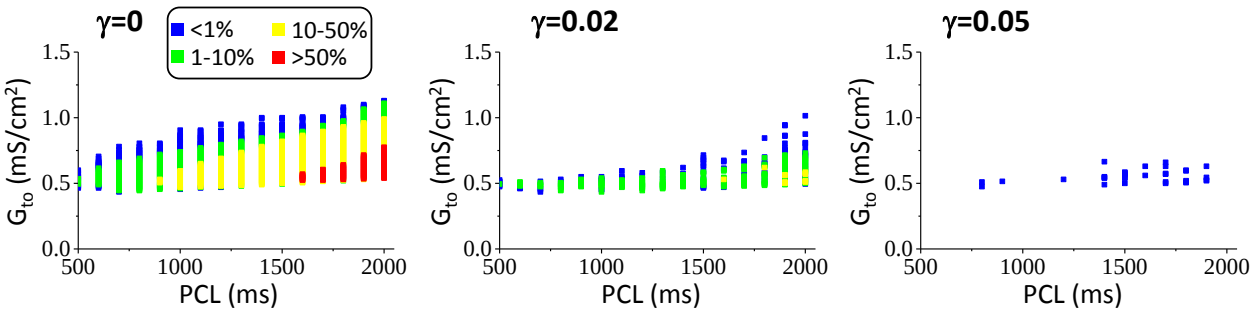

Figure VI. Dependence of P2R on heart rate and late I_{to} for the ten Tusscher et al human AP model. 1D cable simulations with periodic pacing the same as for Fig.3A. Percentage of beats exhibiting PVCs versus in G_{to} and PCL for $\gamma = 0$, $\gamma = 0.02$, and $\gamma = 0.05$. 200 pacing beats were applied for each combination of G_{to} and PCL. Color scale indicates the percentage of PVC beats.

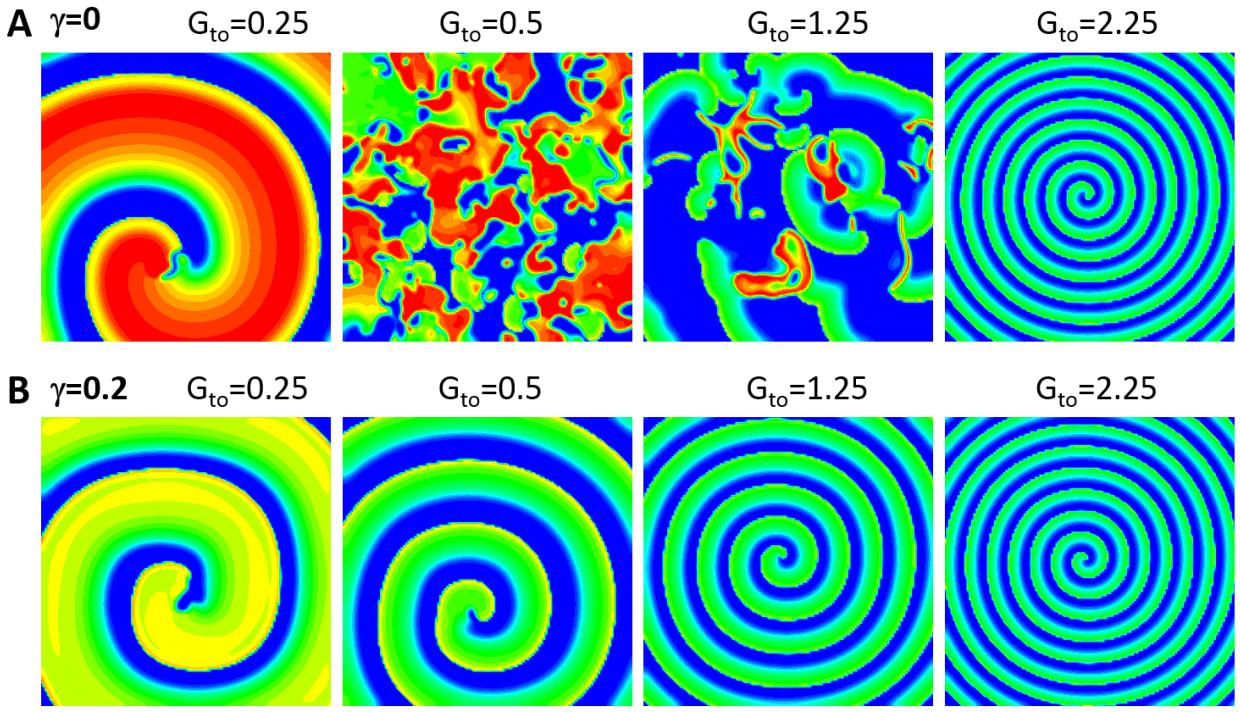

Figure VII. Effects of late I_{to} on reentry stability in 2D homogeneous tissue with the ten Tusscher et al human AP model. Simulations were done in the same way as for Fig.4. **A**. Voltage snapshots for different G_{to} (in unit mS/cm^2) for $\gamma = 0$. Supplemental Movies III and IV show the wave dynamics for G_{to}=0.5 and G_{to}=1.25 mS/cm^2, respectively. **B**. Same as A but for $\gamma = 0.2$.

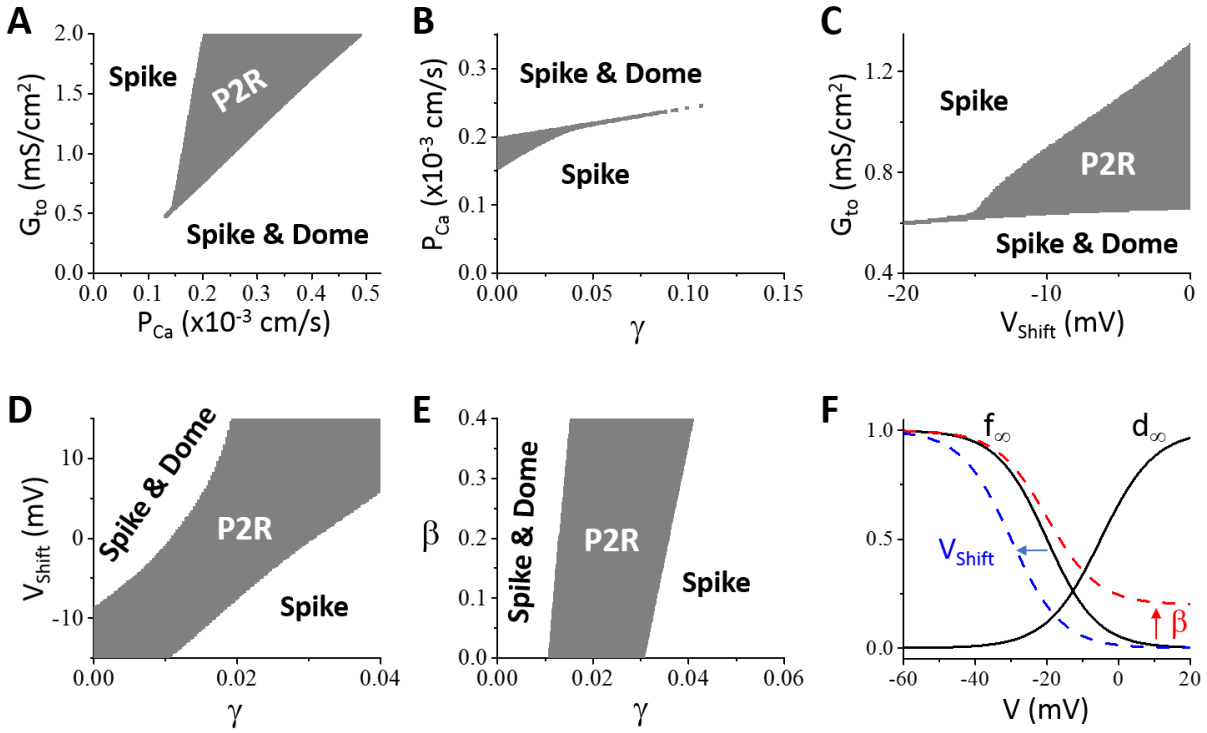

Figure VIII. Effects of $I_{Ca,L}$ on P2R in 1D cable using the ten Tusscher et al human AP model. The cable model is the same as for Fig.6 in main text except the action potential model. **A**. P2R region versus P_{Ca} and G_{to} for $\gamma = 0$. P_{Ca} is a parameter proportional to the maximum conductance of $I_{Ca,L}$. **B**. P2R region versus γ and P_{Ca} for G_{to}=0.75 mS/cm^2. **C**. Effects of window $I_{Ca,L}$ on P2R, simulated by shifting f_∞ as indicated in panel F. Shown is the P2R region versus V_{shift} and G_{to}. **D**. P2R region versus γ and V_{shift}. P_{Ca}=0.00020125 cm/s and G_{to}=0.75 mS/cm^2. **E**. P2R region versus γ and β. β is the parameter controlling the late component of $I_{Ca,L}$ by changing the steady-state inaction (f_∞) as: $f_{\infty,new} = \beta + (1-\beta)f_\infty$ (as indicated in panel F). P_{Ca}=0.00020125 cm/s and G_{to}=0.75 mS/cm^2. **F**. Changes of f_∞. Solid black curve is the original f_∞. Dashed red curve is the one after the late component elevated. Dashed blue curve is the one after a left shift. V_{shift}>0 for the right shift and V_{shift}<0 for the left shift. The results shown in A-E are almost the same as those for the 1994 Luo and Rudy AP model shown in Fig.6 in the main text and in Fig.S4.

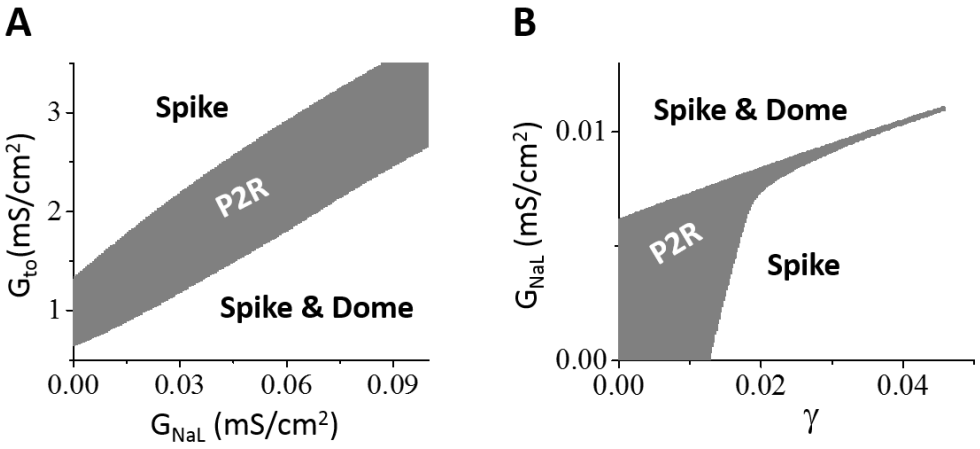

Figure IX. Effects of late I_{Na} on P2R in the 1D cable using the ten Tusscher et al human AP model. The cable model is the same as for Fig.7 in main text except the action potential model. **A**. P2R region versus G_{NaL} and G_{to}. **B**. P2R region versus γ and G_{NaL}. G_{to}=0.75 mS/cm^2. These results are the same as those for the 1994 Luo and Rudy model shown in Figs. 7 C and D in the main text.

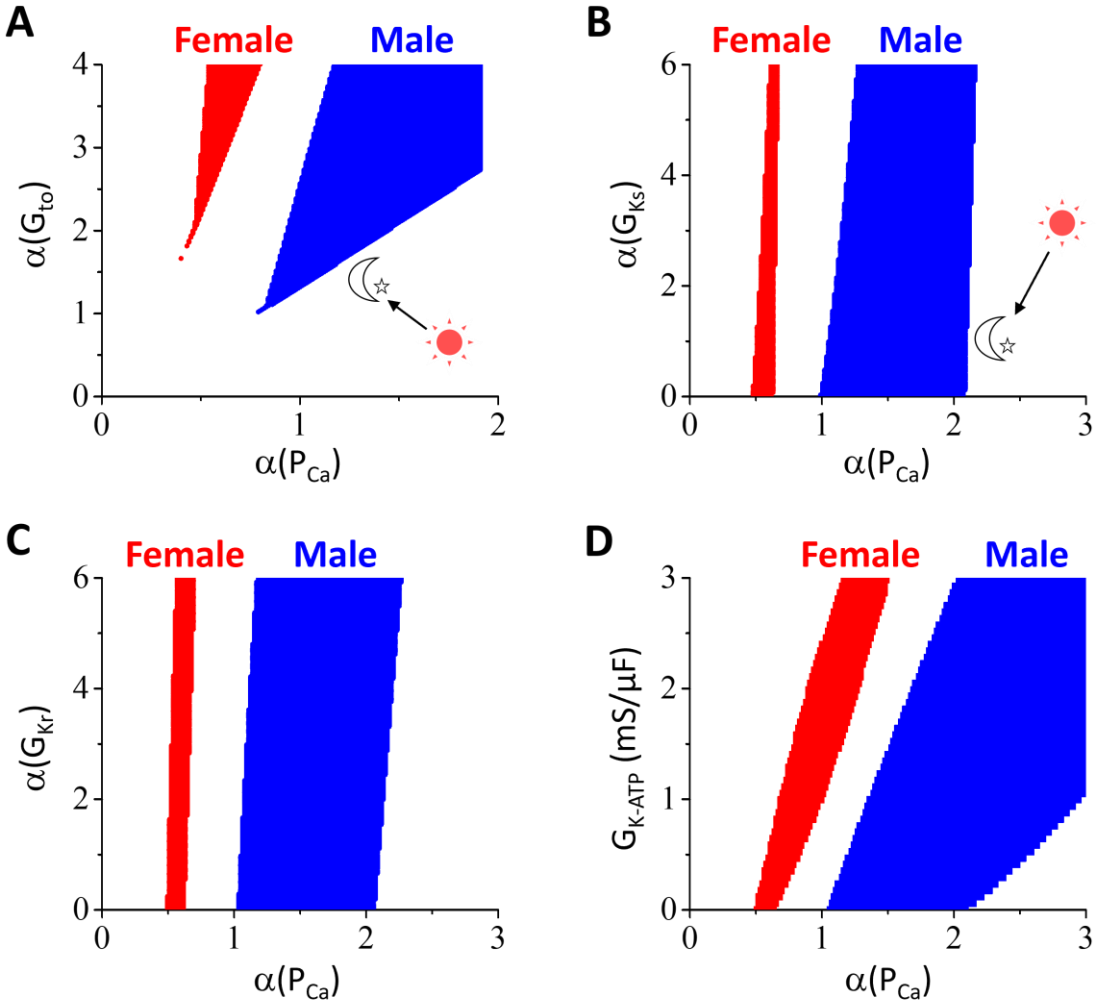

Figure X. Effects of sex difference and circadian rhythm on P2R using the ten Tusscher et al human AP model. Simulations were done in a 1D cable the same way as for Fig.8 in the main text but with the ten Tusscher et al human AP model. **A**. P2R regions for male and female versus $\alpha(P_{Ca})$ and $\alpha(G_{to})$. **B**. P2R regions for male and female versus $\alpha(P_{Ca})$ and $\alpha(G_{Ks})$. **C**. P2R regions for male and female versus $\alpha(P_{Ca})$ and $\alpha(G_{Kr})$. **D**. P2R regions for male and female versus $\alpha(P_{Ca})$ and $G_{K\text{-}ATP}$. $\alpha(G_{to})$=3 was used for B-D.

Supplemental Movies

Movie I. Wave dynamics showing the genesis of P2R in 2D tissue with the 1994 Luo and Rudy model, corresponding to Fig.1C.

Movie II. Wave dynamics showing the genesis of P2R in 2D tissue with the 2004 ten Tusscher et al human model, corresponding to Supplemental Fig.VC.

Movie III. Wave dynamics in 2D homogeneous tissue with the 2004 ten Tusscher et al human model, corresponding to the G_{to}=0.5 mS/cm^2 case in Supplemental Fig.VIIA.

Movie IV. Wave dynamics in 2D homogeneous tissue with the 2004 ten Tusscher et al human model, corresponding to the G_{to}=1.25 mS/cm^2 case in Supplemental Fig.VIIA.